JOURNAL OF THERMOPHYSICS AND HEAT TRANSFER
Vol. 8, No. 4, Oct.–Dec. 1994

Measurement and Analysis of Nitric Oxide Radiation in an Arcjet Flow

Dikran S. Babikian,* Nigel K. J. M. Gopaul,† and Chul Park‡
NASA Ames Research Center, Moffett Field, California 94035

Radiation from the nitric oxide (NO) band systems emitted by the flow in the test section of a 20-MW arcjet wind tunnel was measured and compared with the computed values for the purpose of testing the validity of an existing thermochemical model. The settling chamber pressure and enthalpy were 2.4 atm and 28 ± 10 MJ/kg, respectively. The measurements were made using photographic films in the wavelength region from 225 to 305 nm. Of the four band systems of NO (beta, gamma, delta, and epsilon), vibrational transitions were observed from only the upper $v' = 0$ levels. Excitation temperatures were deduced by comparing the experimental spectrum with those calculated using the nonequilibrium radiation code NEQAIR. The rotational, vibrational, and electronic excitation temperatures deduced from the data were $T_r = 560 \pm 50$ K, $T_v \leq 950 \pm 50$ K, and $T_{ex} = 11{,}500 \pm 520$ K, respectively. A multitemperature nonequilibrium nozzle flow code NOZNT was used to calculate the nozzle flow. The calculated temperatures were $T_r = 560$ K, $T_v = 950$ K, and electron thermal temperature $T_e = 6100$ K, respectively at 30 MJ/kg. The presented results show that by using the centerline enthalpy value deduced from heat transfer measurement and the NOZNT code, one can predict the freestream conditions in an arcjet wind-tunnel flow fairly well.

Nomenclature

A = cross-sectional area of nozzle, m^2
H = enthalpy, MJ/kg
I = intensity of a spectral line, W/(cm^2-μ-sr)
T = heavy particle translational temperature, K
T_e = electron translational temperature, K
T_{ex} = electron excitation temperature, K
T_r = rotational temperature, K
T_v = vibrational temperature, K
v = vibrational quantum number
x = distance from throat, m

Subscripts
a = mass averaged
i = species index

Superscripts
$*$ = throat
$'$ = upper state

Introduction

FOR the last three decades arcjet wind tunnels have been used to simulate the high enthalpy environments encountered during hypervelocity atmospheric entry of space vehicles. The heat shields of all such vehicles, including those for the Apollo and the Space Shuttle vehicle, have been developed by testing in arcjet wind tunnels.

Testing of heat shield materials will become even more critical for the proposed Mars mission because the entry velocity will be higher than those for the past missions. In spite of the importance of the arcjet facilities, the aerothermodynamic states of the flows produced in them are not yet well understood. This is due to the complexity of the physical and chemical phenomena occurring in these facilities. The flow undergoes vibrational excitation, dissociation, and ionization. Because of the relatively low density environment produced in the facility, it is generally in nonequilibrium in both chemical composition and internal modes.

There have been some efforts to characterize the arcjet flows by using the available experimental and computational techniques.[1,2] Despite such efforts, many uncertainties still exist. In particular there has not been a measurement of vibrational or electronic temperatures of nitric oxide (NO). These temperatures of NO are important because NO plays an important role in the chemistry of the nozzle flows.[3]

The objectives of the present work are to experimentally characterize the behavior of NO and to explore whether it can be numerically reproduced. Radiation from NO was measured in the test section stream of a 20-MW arcjet wind tunnel at NASA Ames Research Center. From the data, we determined its rotational, vibrational, and electronic excitation temperatures that are consistent with the limited data. The results of the measurements were compared with the theoretical calculations. These calculations included the computation of arc constrictor flow, nozzle flow, and nonequilibrium radiation. Due to the complex nature of the flow in the settling chamber, accurate prediction of the flow properties in this chamber remains uncertain and is under investigation.[4] The calculated temperatures and the synthetic radiation spectrum are generally in fair agreement with the measurements.

Experiment

Test Conditions and Experimental Setup

The arc heater of the 20-MW arcjet wind tunnel at NASA Ames Research Center used in the present work (Aerodynamic Facility) consists of a constrictor tube that is 216 cm long with a 6 cm i.d. The constrictor is followed by a settling chamber 10.4 cm in diam and 25.6 cm in length. From the

Presented as Paper 93-2800 at the AIAA 28th Thermophysics Conference, Orlando, FL, July 6–9, 1993; received Aug. 12, 1993; revision received March 14, 1994; accepted for publication March 28, 1994.

*Senior Research Scientist, Thermosciences Institute, M/S 230-2. Member AIAA.
†Research Scientist, Thermosciences Institute. Member AIAA.
‡Staff Scientist. Associate Fellow AIAA.

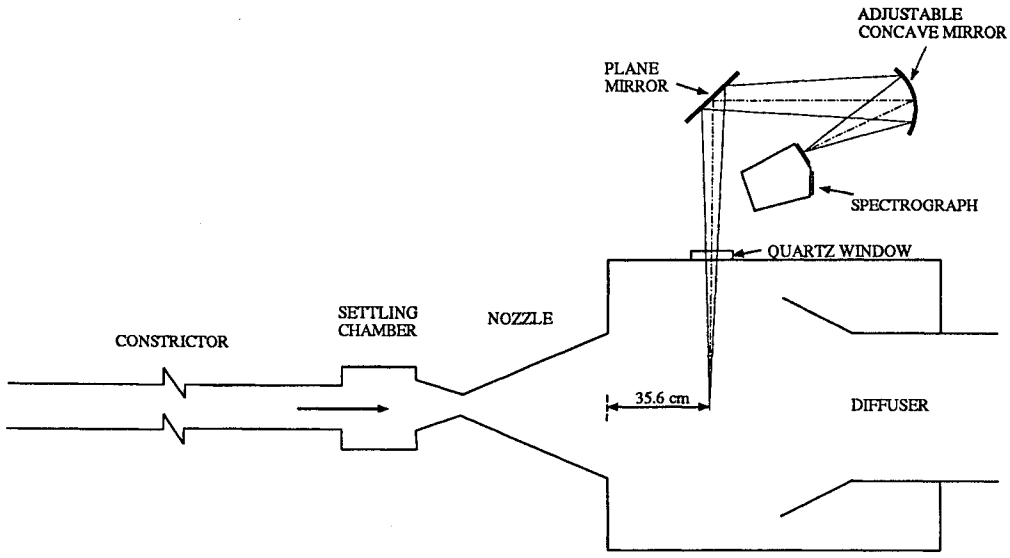

Fig. 1 Schematic drawing of the experimental setup.

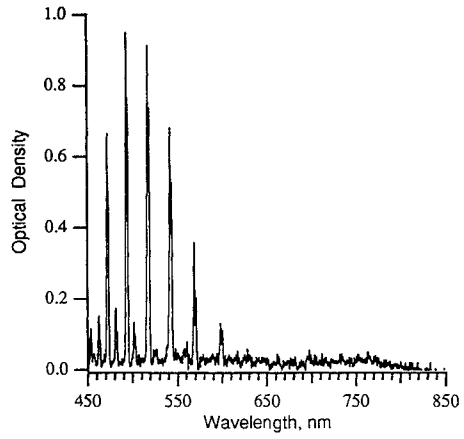

Fig. 2 Densitometer trace of the 450–850-nm (first order) spectral range.

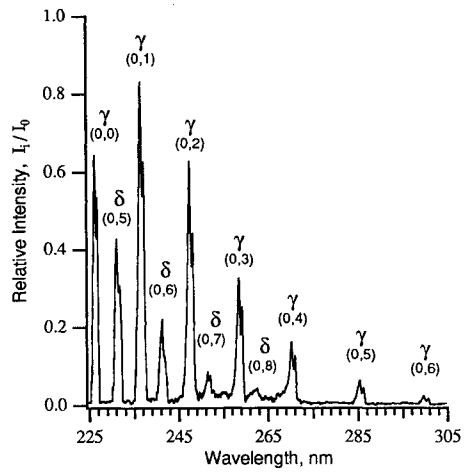

Fig. 3 Corrected intensity trace of the 225–305-nm spectral range.

settling chamber the flow is expanded through a convergent-divergent nozzle of throat diameter 3.81 cm, to an exit diameter of 45.72 cm with an 8-deg half-angle and an area ratio of 130.

The arc heater was operated with a settling chamber pressure of 2.4 atm, a flow rate of 0.0864 kg/s, electric current of 2000 A, and a voltage of 2600 V. The test gas consisted of 87% air and 13% argon by mass. The average value of the flow enthalpy based on heat balance measurements, i.e., electrical energy input minus the energy lost in the cooling water divided by the mass flow rate, was 22 MJ/kg. The flow enthalpy at the nozzle centerline based on heat transfer rate measurements to a spherical blunt body[5] was 28 MJ/kg.

Spectral data were obtained in the freestream flow 35.6 cm downstream of the nozzle exit. The measurements were made photographically because the radiation signal was too weak, due to the low density nature of the expanding flow, to be measured reliably with photoelectric method while maintaining a sufficiently high wavelength resolution. A McPherson spectrograph model 218 with a small f-number and a short focal length was used to collect the data. The spectrograph has an f-number of 5.3 and a focal length of 0.3 m. This spectrograph is known as a criss-crossed Czerny-Turner optical system.[6] It is an unconventional mounting arrangement where the light beam from the two mirrors and the plane grating are crossed in order to obtain a low f-number. The signal was recorded on a film on this instrument by an exposure of 30 s. A Joyce Loebel microdensitometer model MK III CS was used to measure the optical densities recorded on a high speed infrared film (HIE). The microdensitometer traces were digitized and transferred to a computer to be calibrated, analyzed, and compared with the theoretical predictions.

Further description of the experimental setup, instrumentation, data collection, and data calibration, are presented in Refs. 7 and 8. Figure 1 shows the schematic sketch of the experimental optical setup.

Experimental Spectra

As can be seen from Fig. 1, the radiation observed by the spectrograph is an integration of the intensity along the optical path across the flowfield. However, since radiation power is generally strongly dependent on the controlling temperatures, and since these temperatures are the highest along the centerline of the nozzle flow, it is likely that the observed spectra are representative of those in the centerline region of the nozzle flow.

The densitometer trace of the record taken in the spectral range 450–850 nm, in the first order, is shown in Fig. 2. The total wavelength resolution was 0.67 nm in first order. The ordinates in the figure represent optical density of the film, i.e., the logarithm of the attenuation of a light beam through the film. According to the spectrum shown in Fig. 2, the only significant radiation emanates from NO gamma and NO delta band systems (in second order).

The measured intensity was corrected for the film response in two steps using a National Bureau of Standards-certified calibrated lamp. First the film was calibrated for the relative intensity at specific wavelengths using neutral density step-wedge filters. Second, the film was calibrated for the film sensitivity, the spectrograph grating, and the entire optical setup against wavelength. However, absolute intensity values were not obtained from the data since film exposures were not made using any standard calibration lamp. Figure 3 shows the corrected relative intensity trace of the NO band systems adjusted to the first order in the 225–305-nm wavelength range.

As indicated in Fig. 3, the spectral bands detected by the spectrograph were identified as the NO gamma and NO delta band systems in second order. The NO gamma band system corresponds to the $A^2\Sigma^+ \rightarrow X^2\Pi$ transition where $A^2\Sigma^+$ is an upper electronic state and $X^2\Pi$ is the ground electronic state of the NO molecule. The NO delta band system is produced by transitions from the $C^2\Pi \rightarrow X^2\Pi$ electronic states. The NO beta band system ($B^2\Pi^+ \rightarrow X^2\Pi$), which is in the same spectral region as the NO gamma band system (see Fig. 4, from Ref. 9), was not present in the recorded spectrum. For both the gamma and delta systems only the vibrational transitions from the upper $v' = 0$ level were present; i.e., (0,1), (0,2), (0,3), etc.

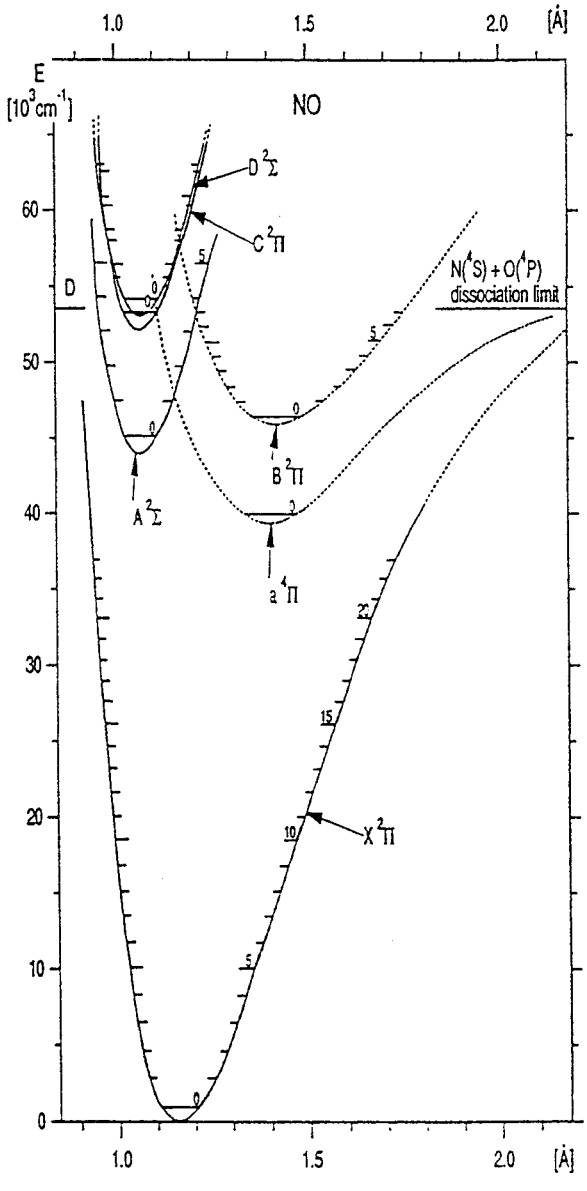

Fig. 4 Selected potential curves of NO molecule.[9]

Temperature Determination

The excitation temperatures of the flowfield were deduced by comparing the relative intensities in the recorded spectra with those calculated in the 225–305-nm range. The radiative emission spectra were computed using the latest modified version of the original nonequilibrium air radiation code NEQAIR.[10] This version, which is at NASA Ames Research Center, introduces the most updated transition probabilities and spectroscopic and radiative constants. It also incorporates the changes reported in Refs. 11–13. The thermochemical model used in the code has been well documented in Refs. 14–17 and therefore will not be described here. The nonequilibrium excitation portion of the code was bypassed by specifying Boltzmann distribution of electronic, vibrational, and rotational excitation modes. This was done to determine the equivalent Boltzmann temperature in the flowfield. Also, the code accounted for the emission and the absorption of each individual specie in determining the intensity. When absorption was excluded from the calculations, intensities remained unchanged, indicating that the flow is optically thin.

The width of a vibrational band is dictated mostly by the rotational temperature of the molecule. In the present work, the rotational temperature was determined from the (0,2) band of the gamma system. The temperature was altered in the calculation until the calculated value of the band width at half its maximum intensity matched that of the experimental spectrum. The rotational temperature so determined was $T_r = 560 \pm 50$ K. The rotational temperatures obtained using other Gamma band systems were within 5% of the value obtained using the (0,2) band system. The source of uncertainty in temperature determination is attributed to the uncertainties about film characteristics such as noise and fog levels in the film.

The ratio of the relative intensity of the delta system to that of the gamma system depends on the electronic excitation temperature governing the two systems. Through a computational process similar to that used for the rotational temperature, an electronic excitation temperature of $T_{ex} = 11{,}500 \pm 520$ K was obtained. In Refs. 7 and 8, T_{ex} was erroneously stated to be 7560 ± 340 K. This error was caused by the use of the old values of intensity parameters (transition moments). To determine the vibrational temperature of NO, radiation from two vibrational levels is needed. However, only bands from $v' = 0$ state were observed in the data. From the fact that the radiation from the $v' = 1$ state of the upper electronic state of NO gamma was absent in the observed spectrum, only the upper limit of the vibrational temperature of NO can be determined. In order for the radiation from the $v' = 1$ state to be equal to or less than the observed noise level, the vibrational temperature was determined to be below 950 ± 50 K. Figures 5a and 5b show the calculated spectra of the radiation emitted by the NO band systems. In Fig. 5a the emission spectrum from the gamma and delta systems is shown. This spectrum is in good agreement with the experimental spectrum shown in Fig. 3. The emission spectrum from the beta and epsilon systems is shown in Fig. 5b. Note that the radiation from these systems is an order of magnitude weaker than that from gamma and delta. Also, the beta and epsilon systems are not present in the recorded spectrum shown in Fig. 3. The absence of the beta band system indicates that the $B^2\Pi$ electronic state is not populated to a significant extent, although it is located at nearly the same energy level as the $A^2\Sigma^+$ state from which the Gamma system emanates (see Fig. 4). The $B^2\Pi$ state has a larger internuclear distance than the $A^2\Sigma^+$ state. The electronic states of the NO molecule may be populated through a selective populating process according to internuclear distance under nonequilibrium.

The upper state of the NO epsilon band system ($D^2\Sigma^+$) lies very close to the upper state of the gamma band system as shown in the energy potential curves in Fig. 4. However, the strong bands of NO epsilon lie in the vacuum uv, and only a

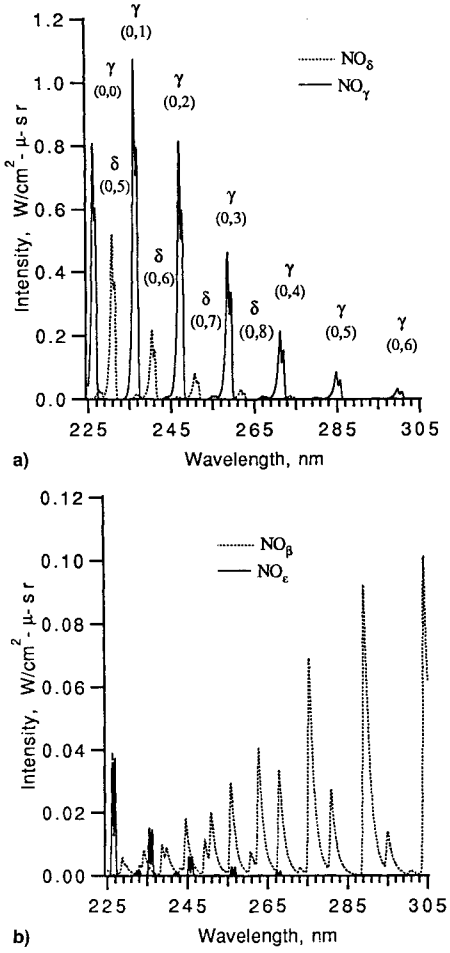

Fig. 5 Calculated spectrum of NO: a) delta and gamma and b) beta and epsilon band systems.

few of the weaker bands are in the spectral region of our experiment. These weak vibrational bands (0,5), (0,6), and (0,7) lie under the much stronger vibrational bands (0,0), (0,1), and (0,2) of the gamma system and their contribution to the measured radiation is insignificant. To verify the existence of NO epsilon in the freestream flow, further emission measurements are needed in the vacuum uv spectral region where the gamma band system does not exist.

Flowfield Calculations

Nozzle Inlet Conditions

In order to carry out the nozzle flow calculations, one must know the conditions at the nozzle entrance. The entrance condition is dictated by the flow processes in the settling chamber. Since the settling chamber receives its flow from the arc constrictor, one must first calculate the constrictor flowfield. The flow conditions at the exit of the constrictor were calculated using the arc heated flowfield code ARCFLO.[18,19] The code assumes the flow to be in thermochemical equilibrium and uses real gas properties.[18,20]

Figure 6 shows radial distributions of velocity, temperature, and enthalpy at the exit of the constrictor. The centerline values were 225 m/s, 12,200 K, and 60 MJ/kg, respectively. The calculated mass averaged total enthalpy at the exit of the constrictor was 22 MJ/kg. The calculated averaged enthalpy value agrees with the value determined from heat balance. However, the calculated centerline enthalpy value is much greater than the value based on heat transfer rate.

The discrepancy between the two centerline enthalpy values is believed to be due to the circulation and mixing between the hot gas in the centerline region and the cold gas in the peripheral region. The resulting distribution of these properties in the settling chamber is difficult to predict, although an effort is presently being made to analyze it.[4] However, because of this phenomenon, it is expected that the distribution of temperature and enthalpy at its exit will be more uniform than that shown in Fig. 6. Therefore, it is reasonable to assume the centerline enthalpy to be in the range of 28 ± 10 MJ/kg.

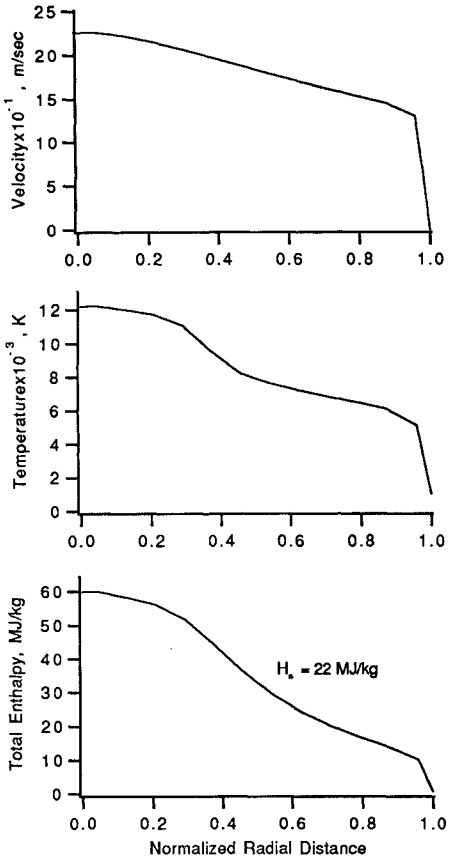

Fig. 6 Calculated radial distribution of velocity, temperature, and enthalpy profiles.

In the present work, calculations were carried out for enthalpy values between 20–60 MJ/kg in an increment of 5 MJ/kg. The value of 30 MJ/kg, which is close to the 28-MJ/kg value deduced from heat transfer measurement, was used as the inlet enthalpy for the nozzle flow calculation.

Nozzle Flowfield

The computer code NOZNT[2,21] was used to calculate the flow along the centerline of the nozzle of the arcjet wind tunnel. The code solves a one-dimensional steady flow through a convergent-divergent nozzle in the dissociated and ionized regime. In the nozzle flow calculations, the nozzle geometry was assumed to be hyperbolic, i.e., conical with a smooth transition at the throat, of the form $A/A^* = 1 + cx^2$. It assumes the entrance and the beginning section of the nozzle to be at equilibrium. The rest of the nozzle is solved assuming multitemperature nonequilibrium flow. The equilibrium portion of the flow is solved with the pressure-specified method.[22]

The nonequilibrium calculations of the flow are started in the converging portion of the nozzle upstream of the throat. The nonequilibrium calculation also uses the pressure-specified method up to the point where the frozen Mach number is 1.8. From this point the area-specified method is used.[2] In this region of the flow the equations of conservation of species, vibrational energy, and electron-electronic energy are solved numerically.

The kinetic model used for the ionized air includes the following reactions: dissociation, neutral exchange, associative ionization, electron-impact ionization, and radiative recombination. The vibrational relaxation parameters and the

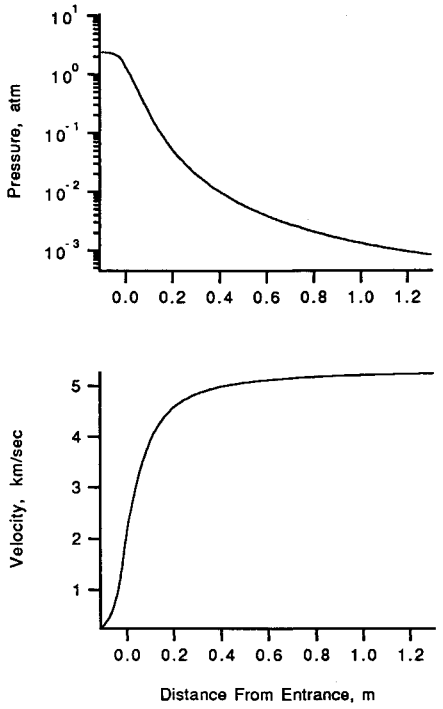

Fig. 7 Calculated velocity and pressure variation along the nozzle axis.

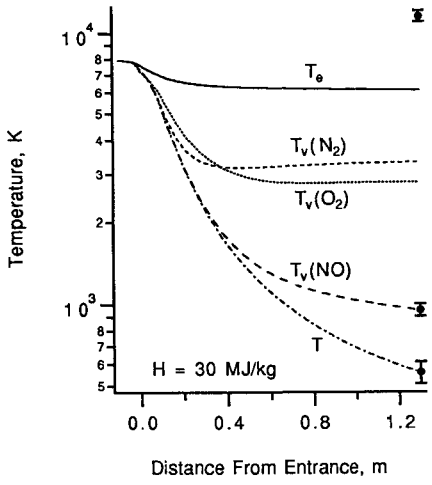

Fig. 8 Calculated excitation temperatures along the nozzle axis.

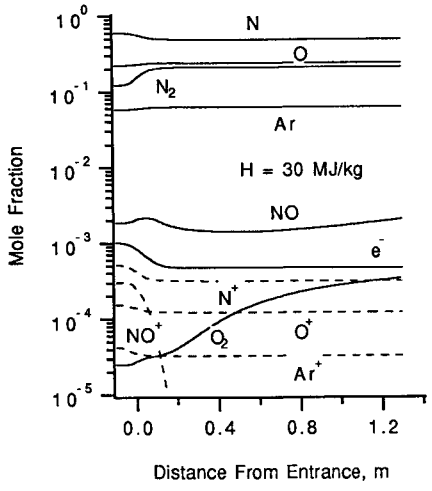

Fig. 9 Calculated mole fractions along the nozzle axis.

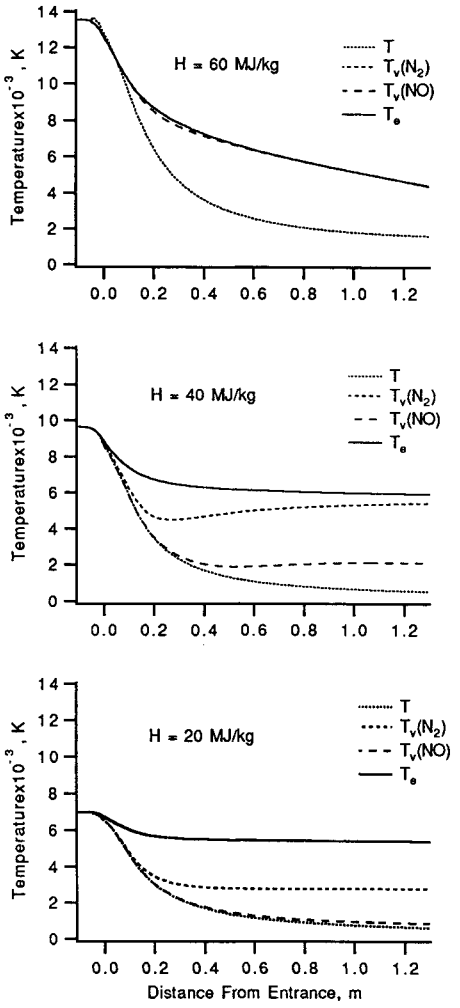

Fig. 10 Effect of inlet enthalpy on nozzle flowfield.

reaction rate coefficients are summarized in Refs. 2 and 23, and therefore they will not be included in this article. Those rate parameters were used in the present work except for those for ionic recombination of N^+ and O^+. Numerical difficulties were encountered for some calculations where enthalpy was higher than 45 MJ/kg. These difficulties disappeared when the ionic recombination rates were multiplied by 10. The increase in ionic recombination rate causes an increase in electronic temperature due to the energy feedback phenomenon. The increase in electron temperature in turn suppresses further recombination. For the cases where there were no numerical difficulties, the change of the rate constants resulted in negligible differences. Since these rate constants are uncertain by about an order of magnitude, the changes are acceptable for the purpose of the present work.

Figure 7 shows the calculated pressure and velocity along the axis of the nozzle. The code assumes that T and T_r are the same. Likewise, T_e and T_{ex} are taken to be the same. This assumption is based on the knowledge that the electrons are very efficient in causing electronic excitation. Therefore, the populations of electronic states tend toward the Boltzmann values dictated by the electron translational temperature. Since there are a large number of electronic states, it is impractical to individually account for the populations of each electronic state.[15,16,24] However, molecular species i are allowed to have different vibrational temperatures T_{v_i}.

Figures 8 and 9 show the temperature and mole fraction profiles along the nozzle axis. At the point where the experimental measurements were made, the calculated temperatures were T_r = 560 K, T_v(NO) = 950 K, and T_e = 6100 K at the enthalpy value of 30 MJ/kg.

Discussion

The excitation temperatures deduced from the experimental spectrum are shown in Fig. 8 by the circle symbols with error bars and are compared with the NOZNT calculation. The figure shows that the calculated translational-rotational and the NO vibrational temperatures are in good agreement with the corresponding experimentally deduced values. The difference between the measured T_{ex} and the calculated T_e may be due to the breakdown of the assumption that the two temperatures are equal. However, both these temperatures, T_e and T_{ex}, are much higher than T_v(NO), and thereby it underscores the need for a multitemperature description of the flow. The vibrational temperature of N_2 was not measured in this experiment. However, the accuracy in the calculated value of $T_v(N_2)$ was verified in Ref. 2 by comparing it with experiments where N_2 vibrational temperature was measured.

In order to examine the sensitivity of calculated temperatures to the uncertainty in the measured arcjet enthalpy, the foregoing calculations were repeated for different values of nozzle entrance enthalpies. Figure 10 shows the effect of inlet enthalpy on the variation of temperatures along the nozzle centerline. As the enthalpy increases from 20 to 60 MJ/kg, the vibrational temperatures tend to equilibrate with electron-electronic temperature. This is caused by the increase in the collision frequency between the electrons and the molecules due to the increase in electron number density. The vibrational temperature of N_2 approaches electron-electronic temperature faster than that of NO because of the large cross section between the vibrational mode of N_2 and electrons.[2] Also note that at high enthalpies all temperatures (translational-rotational, vibrational, electron-electronic) tend to equilibrate as expected.

As the enthalpy increased from 20 to 60 MJ/kg, the translational-rotational temperature increased from 550 to 1500 K. However, the electron temperature reached a maximum value of 6200 K at $H = 35$ MJ/kg, and decreased thereafter as the enthalpy increased further. At enthalpies greater than 45 MJ/kg the electronic temperature and all vibrational temperatures are in equilibrium, whereas at enthalpies below 25 MJ/kg the translational temperature and the NO vibrational temperature are in equilibrium.

The value of T_v(NO) found in the present experiment indicates that the enthalpy is below 35 MJ/kg. A previous work[25] indicates that the enthalpy value deduced from the heat transfer measurement tends to underestimate the enthalpy in typical arcjet conditions. Therefore, the enthalpy is most likely between 28 MJ/kg, the value determined from the heat transfer measurement, and 35 MJ/kg. It is to be noted that at the enthalpy of 60 MJ/kg, which is the value of the enthalpy at the constrictor centerline, the concentration of NO is very small and it is unlikely that its radiation could be observed experimentally.

As shown in Ref. 25, enthalpy can be best determined spectroscopically by observing radiation emitted from the shock layer formed in front of a blunt body. Such an effort is currently in progress. Measurements of the spectral radiation (120–900 nm) incident on the stagnation region surface of a blunt body in the test section have been made,[26,27] and the analysis described in this article is being extended to include the shock layer modeling. Preliminary predictions of the incident radiation spectrum have been made and are being compared with the experimental data.[28] Results of this analysis will be used to define future arcjet tests to continue development of arcjet wind-tunnel modeling. A validated model of these facilities will help design advanced arcjets and extend their usefulness as aerothermodynamic testing facilities.

Conclusions

The presented results show that by using the centerline enthalpy value deduced from heat transfer measurement and the NOZNT code, one can predict the freestream conditions in an arcjet wind-tunnel flow fairly well. The translational-rotational temperature and the vibrational temperature of NO can be closely reproduced by NOZNT. The calculated electron-electronic temperature T_e is appreciably lower than the measured electronic excitation temperature T_{ex} of NO. Compared with the electron and electronic temperatures, the vibrational temperature of N_2 and NO are significantly lower at enthalpies less than 45 MJ/kg. In the same enthalpy range, the vibrational temperature of NO is significantly lower than that of N_2. The enthalpy deduced from the spectroscopic measurements agrees approximately with that deduced from heat transfer measurement.

Acknowledgments

This work was supported partially by a NASA Ames Director's Discretionary fund. The support for D.S.B. by NASA Grant NCC2-420 to the Eloret Institute, Palo Alto, California, is gratefully acknowledged.

References

[1]Scott, D. C., "Survey of Measurements of Flow Properties in Arcjets," *Journal of Thermophysics and Heat Transfer*, Vol. 7, No. 1, 1993, pp. 9–23.

[2]Park, C., and Lee, S. H., "Validation of Three-Temperature Nozzle Flow Code NOZNT," AIAA Paper 93-2862, July 1993.

[3]Olenberg, R., Chinitz, W., Friedman, M., Jaffe, R., Jachimowski, C., Rabinowitz, M., and Scott, G., "Hypersonic Combustion Kinetics: Status Report of the Rate Constant Committee, NASP High Speed Propulsion Technology Team," NASP Rate Constant Committee, NASP TM-1107, 1990.

[4]Durgapal, P., and Palmer, G., "Strongly Coupled Radiative Transfer and Joule Heating in the Cathode of an Arc Heater," AIAA Paper 93-2801, July 1993.

[5]Winovich, W., Buboni, J., and Balakrishnan, A., "Application of Numerical Simulation to Enhance Arc-Jet Performance Simulation," *Thermophysical Aspects of Reentry Flows*, edited by J. N. Moss and C. D. Scott, Vol. 103, Progress in Astronautics and Aeronautics, AIAA, New York, 1986, pp. 393–415.

[6]McPherson Instruments, *Instruction Manual for Model 218, 0.3 Meter Combination Scanning Monochromator and Spectrograph*, Acton, MA, 1975.

[7]Gopaul, N. K. J. M., "Spectral Measurement of Nonequilibrium Nitric Oxide in the Free-Stream of an Arc-Jet Flow," M.S. Thesis, Stanford Univ., Stanford, CA, 1992.

[8]Gopaul, N. K. J. M., "Spectral Measurement of Nonequilibrium Arc-Jet Free-Stream Flow," Instrument Society of America, ISA Paper 93-144, May 1993.

[9]Scheingraber, H., and Vidal, C. R., "Flourescence Spectroscopy and Frank-Condon Factor Measurements for Low-Lying NO Rydberg States," *Journal of the Optical Society of America*, Pt. B, Vol. 2, No. 2, 1985, pp. 343–354.

[10]Park, C., "Nonequilibrium Air Radiation (NEQAIR) Program: User's Manual," NASA TM 86707, July 1985.

[11]Moreau, S., Laux, C. O., Chapman, D. R., and MacCormack, R. W., "A More Accurate Nonequilibrium Air Radiation Code: NEQAIR Second Generation," AIAA Paper 92-2968, July 1992.

[12]Laux, C. O., Gessman, R. J., and Kruger, C. H., "Modeling the UV and VUV Radiative Emission of High-Temperature Air," AIAA Paper 93-2802, July 1993.

[13]Laux, C. O., "Optical Diagnostics and Radiative Emission of Air Plasma," Ph.D. Dissertation, Stanford Univ., Stanford, CA, 1993.

[14]Park, C., "Calculation of Nonequilibrium Radiation in the Flight Regimes of Aeroassisted Orbital Transfer Vehicles," *Thermal Design of Aeroassisted Orbital Transfer Vehicles*, edited by H. F. Nelson, Vol. 96, AIAA, Progress in Astronautics and Aeronautics, New York, 1985, pp. 395–418.

[15]Park, C., "Assessment of Two-Temperature Kinetic Model for Dissociating and Weakly-Ionizing Nitrogen," *Journal of Thermophysics and Heat Transfer*, Vol. 2, No. 1, 1988, pp. 8–16.

[16]Park, C., "Assessment of Two-Temperature Kinetic Model for Ionizing Air," *Journal of Thermophysics and Heat Transfer*, Vol. 3, No. 3, 1989, pp. 233–244.

[17]Whiting, E. E., and Park, C., "Radiative Heating at the Stagnation Point of the Aeroassisted Flight Experiment Vehicle," NASA TM 102829, Nov. 1990.

[18]Watson, V. R., and Pegot, E. B., "Numerical Calculations for the Characteristics of Gas Flowing Axially Through a Constricted Arc," NASA TN D-4042, June 1967.

[19]Nicolet, W. E., Shepard, C. E., Clark, K. C., Balakrishnan, A., Kesselring, J. P., Suchsland, K. E., and Reese, J. J., "Methods for the Analysis of High-Pressure, High-Enthalpy Arc Heaters," AIAA Paper 75-704, May 1975.

[20]Stine, H. A., and Watson, V. R., "The Theoretical Enthalpy Distribution of Air in Steady Flow Along the Axis of a Direct-Current Electric Arc," NASA TN D-1331, Aug. 1962.

[21]Park, C., and Babikian, D. S., "User's Manual for NOZNT and NOZ1T, Nozzle in *n*-Temperature and Nozzle in One Temperature," NASA TN, Aug. 1993, in review.

[22]Lordi, J. A., Mates, R. E., and Moselle, J. R., "Computer Program for the Numerical Solution of Nonequilibrium Expansions of Reacting Gas Mixture," NASA CR-472, May 1966.

[23]Park, C., "Review of Chemical-Kinetic Problems of Future NASA Missions, I: Earth Entries," *Journal of Thermophysics and Heat Transfer*, Vol. 7, No. 3, 1993, pp. 385–398.

[24]Park, C., *Nonequilibrium Hypersonic Aerothermodynamics*, Wiley, New York, 1990.

[25]Okuno, A. F., and Park, C., "Stagnation-Point Heat-Transfer Rate in Nitrogen Plasma Flows: Theory and Experiment," *Journal of Heat Transfer*, Vol. 92, Ser. C, No. 3, 1970, pp. 372–384.

[26]Palumbo, G., Craig, R., and Carrasco, A., "Spectral Measurements of Shock Layer Radiation in an Arc-Jet Wind Tunnel," Instrument Society of America, ISA Paper 93-145, May 1993.

[27]Craig, R., Palumbo, G., and Carrasco, A., "VUV Shock Layer Radiation in an Arc-Jet Wind Tunnel Experiment," NASA TM 108796, 1994.

[28]Babikian, D. S., Palumbo, G., Craig, R., Park, C., Palmer, G., and Sharma, P. S., "Measured and Calculated Spectral Radiation from a Blunt Body Shock Layer in an Arc-Jet Wind Tunnel," AIAA Paper 94-0086, Jan. 1994.